energies

MDPI

Article

Influence of Cooling Water Parameters on the Thermal Performance of the Secondary Circuit System of a Modular High-Temperature Gas-Cooled Reactor Nuclear Power Plant

Xin Wang [1], Gang Zhao [1], Xinhe Qu [1,*], Xiaoyong Yang [1], Jie Wang [1] and Peng Wang [2]

[1] Institute of Nuclear and New Energy Technology, Advanced Nuclear Energy Technology Cooperation Innovation Center, Key Laboratory of Advanced Reactor Engineering and Safety of Ministry of Education, Tsinghua University, Beijing 100084, China; xin-wang21@mails.tsinghua.edu.cn (X.W.); zhaogang88@mail.tsinghua.edu.cn (G.Z.); xy-yang@tsinghua.edu.cn (X.Y.); wjinet@tsinghua.edu.cn (J.W.)
[2] State Nuclear Electric Power Planning, Design & Research Institute Co., Ltd., Beijing 100095, China; wangpeng@snpdri.com
* Correspondence: qxh2018@mail.tsinghua.edu.cn

Abstract: This study quantitatively analysed the influence of cooling water parameters on the performance of a modular high-temperature gas-cooled reactor (MHTGR) nuclear power plant (NPP). The secondary circuit system and cold-end system were modelled using EBSILON software, version 16.0. The influence of cooling water inlet temperature and mass flow rate on the thermal performance of the secondary circuit system was analysed over the full power range with the goal of optimising net power. Under 100% rated condition, for each 1 °C increase in cooling water inlet temperature between 10 and 33 °C, the net power and cycle efficiency decreased by 0.67 MW and 0.14%, respectively, whereas the heat consumption rate increased by 28.72 kJ/(kW·h). The optimal cooling water mass flow rates corresponding to cooling water inlet temperatures of 16 °C and 33 °C were obtained. The optimal cooling water mass flow rate decreased nonlinearly with decreasing power levels. At a cooling water inlet temperature of 33 °C, an increase in cooling water mass flow rate from the designed value (7697.61 kg/s) to the optimal value (10,922.14 kg/s) resulted in a 1.03 MW increase in net power. These findings provide guidelines for MHTGR NPP operation optimisation and economic improvement, especially under high-temperature weather conditions.

Keywords: modular high-temperature gas-cooled reactor; condenser; cooling water; high-temperature weather; EBSILON software

Citation: Wang, X.; Zhao, G.; Qu, X.; Yang, X.; Wang, J.; Wang, P. Influence of Cooling Water Parameters on the Thermal Performance of the Secondary Circuit System of a Modular High-Temperature Gas-Cooled Reactor Nuclear Power Plant. *Energies* **2023**, *16*, 6560. https://doi.org/10.3390/en16186560

Academic Editor: Roman Vadimovich Davydov

Received: 31 July 2023
Revised: 31 August 2023
Accepted: 2 September 2023
Published: 12 September 2023

1. Introduction

The modular high-temperature gas-cooled reactor (MHTGR) belongs to the category of very high-temperature reactor (VHTR), which is one of six advanced reactor types for generation IV nuclear energy systems [1]. Owing to its inherent safety and higher core outlet temperature (700–950 °C), MHTGR is suitable for high-efficiency power generation and a variety of process heat applications [2–7]. The cold-end system [8–10] is an important section of an MHTGR nuclear power plant (NPP). This system is used to cool exhaust steam into condensate and discharge waste heat into the external environment, which determines the final parameters of the steam Rankine cycle. The cold-end system of the Chinese MHTGR NPP adopts an open-loop design method using seawater as the cooling water and the ocean as the final heat sink [2]. After passing through the condenser, the seawater is redischarged into the external environment; it thus undergoes only one cycle. Cooling water parameters such as inlet temperature and mass flow rate affect the performance of the cold-end system, which in turn affects the thermal performance of the secondary circuit system of an NPP.

With the frequent occurrence of extreme high-temperature weather in recent years, the inlet temperature of the cooling water in NPPs has received increasing attention. In

May 2022, Electricite de France (EDF) stated that excessive cooling water (river water) inlet temperatures may reduce the power generation of NPPs in France [11]. Owing to various factors, including high-temperature weather, the EDF's nuclear power generation in the third quarter of 2022 was 55.1 TWh, a decrease of 36.3% compared with that of the third quarter of 2021 [12]. The influence of the cooling water inlet temperature on the thermal performance of NPPs has been studied. Laskowski et al. [13] used EBSILON software to establish a simulation model for a boiling water reactor NPP. The simulation results showed that when the cooling water temperature rose from 10 °C to 28 °C, the plant's total output power decreased by 91.405 MW, and the total efficiency decreased by 2.773%. Attia [14] established a mathematical model for a typical NPP secondary circuit system and performed an energy analysis. The results showed that the system thermal efficiency and output power decrease by 0.152% and 0.444%, respectively, when the cooling water inlet temperature increases by 1 °C. Durmayaz et al. [15] studied the influence of the cooling water inlet temperature on the thermal performance of a conceptual pressurised water reactor NPP in combination with climate conditions in Turkey. This study offers valuable insights into the site selection of power plants.

The cooling water mass flow rate also plays a crucial role in optimising the operation of steam turbine units [16–18]. In a power plant, adjusting the blade angle or the rotational speed of the pump rotor can alter the mass flow rate of cooling water entering the condenser [19–21]. Zhang et al. [22] developed a coupling algorithm using a genetic algorithm–back propagation neural network and a heat transfer model for components of cold-end systems. They determined the optimal mass flow of cooling water for a 350 MW unit at different ambient temperatures. Laskowski et al. [23] approached the optimisation goal from the perspective of the second law of thermodynamics, aiming to minimise the system's entropy generation rate. They obtained a series of optimum cooling water mass flow rates for varying conditions of the power plant. Wu et al. [24] studied a 660 MW thermal power-generating unit under various loads. The optimal cooling water mass flow rates were calculated. The results demonstrated a nonlinear trend, in which the optimal mass flow rate gradually decreased with diminishing load. Błaszczyk et al. [25] focused on choosing the appropriate cooling water mass flow rate for marine power units.

Laskowski et al. [26] analysed the effect of different cooling water mass flow rates on the thermal performance of a 225 MW thermal power plant in Poland within the load range of 40% to 100%. This study revealed that within a certain range, an increment in the cooling water mass flow rate led to an increment in overall power generation; however, it also resulted in a rapid increase in electricity usage by the cooling water pumps. They concluded that when optimising the unit's power output, it is advisable to reduce the cooling water mass flow rate when the unit load falls below 60%.

Most of the existing literature considers thermal power plants and light water reactor NPPs as research objects to examine the influence of cooling water parameters on the thermal performance of power plants. However, there is no research on MHTGR NPPs in the literature. Among the studies that have been conducted, the selected range of cooling water inlet temperature variations is generally limited, and the adverse effects of high-temperature cooling water on plant operations have not been fully considered. Additionally, considering the involvement of MHTGR NPPs in peak load regulation after grid connection, the influence of cooling water parameters over the full power range of NPP operation has to be analysed.

In this study, an energy analysis of the secondary circuit system of an MHTGR NPP was conducted. The construction, as well as verification of the system model, was completed using EBSILON software. Quasi-steady-state simulations were performed within the range of 30% to 100% rated conditions (RC) to quantitatively analyse the impact of varying cooling water parameters on the thermal performance of both the cold-end and secondary circuit systems. The maximum net power was selected as the optimisation goal, and the optimisation function of the EBSILON software was employed to determine the optimal mass flow rate of cooling water for various power levels of the power plant. Furthermore,

at 100% RC, the corresponding optimal cooling water mass flow rates for different cooling water inlet temperatures were obtained. The results provide a basis for evaluating the impact of high-temperature weather on the thermal performance of power plants. Moreover, they can serve as a reference for MHTGR NPPs to optimise their cold-end systems.

2. Model and Validation

2.1. Description of the Model

The secondary circuit system of an MHTGR NPP was used as the research object. It included two steam generators, a steam turbine, a deaerator, two parallel high-pressure (HP) regenerative heaters, three low-pressure (LP) regenerative heaters, pumps, and other components (Figure 1). The first and second circuits of the NPP use helium and water as coolants, respectively. The nuclear island of the plant is equipped with two reactor modules, which provide heat to two steam generators and heat the main feed water into superheated steam. After mixing in the main steam header, the main steam from the two steam generators is directed to the steam turbine. The steam turbine consists of an HP cylinder and two LP cylinders. The arrangement of the LP cylinders follows a dual-flow reverse configuration. Two steam extraction points (I and II) in the HP cylinder provide steam to the HP heaters and deaerator, respectively. The steam extracted from point I is divided into two parts that enter the two parallel HP heaters. The LP cylinders are equipped with three steam extraction points (III, IV, and V), which provide steam for the three LP heaters. Pumps A and B are the two main feed water pumps, pump C is the condensate pump and pumps D and E are the two cooling water pumps.

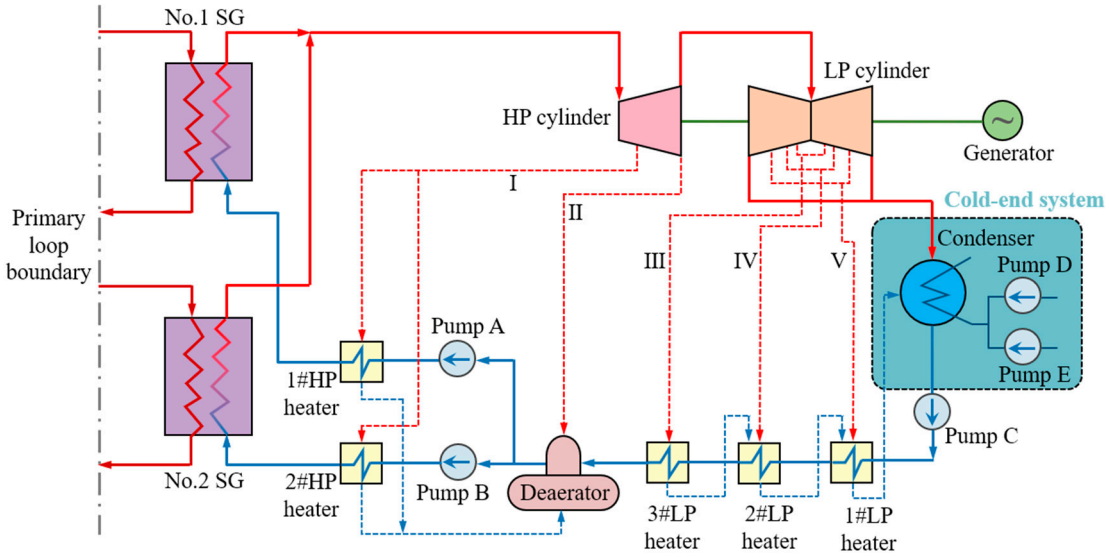

Figure 1. Schematic diagram of the secondary circuit system of the MHTGR NPP.

Table 1 presents the key parameters of the system at 100% RC. According to the design requirements, the minimum power level required for the system to maintain stable operation was 30% RC. Therefore, the power variation range selected in this study was 30–100% RC.

Table 1. Key parameters of the system at 100% RC.

Parameter	Unit	Value
Thermal power of reactor module	MW_{th}	250
Number of reactor modules	-	2
Main steam temperature	°C	566
Main steam pressure	MPa	13.24
Main feed water temperature	°C	205
Condenser back pressure	kPa	4.5

The cold-end system is an important section of NPPs, and the condenser is its core component. As indicated within the dashed box on the right side of Figure 1, the cold-end system of an MHTGR NPP mainly includes a condenser and two cooling water pumps. The condenser is a single-shell, double-pass, tube-and-shell heat exchanger arranged under the steam turbine. The exhaust steam enters from the top of the condenser and condenses into liquid water outside the coolant tubes, which then flows towards the condensate pump [2]. The local seawater, possessing a density of 1023.3 kg/m^3, is selected as the cooling water. The design value of the cooling water inlet temperature is 16 °C. Figure 2 shows a schematic diagram of the condenser. To ensure safety, the two cooling water pumps must operate simultaneously when the power plant operates.

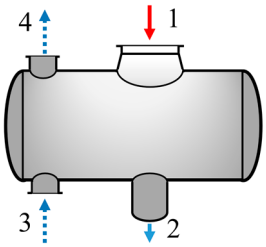

Figure 2. Schematic diagram of the condenser. 1—steam inlet; 2—condensate outlet; 3—cooling water inlet; 4—cooling water outlet.

To calculate the total heat transfer coefficient of the condenser under various operating conditions, the HEI10 (Heat Exchange Institute 10th Edition) method was selected in EBSILON software. Table 2 presents some of the condenser's design parameters, which are indispensable for the modelling process.

Table 2. Some design parameters of the condenser [2,27].

Item	Unit	Value
Tube material	-	titanium
Heat transfer surface area	m^2	12,000
Tube outer diameter	mm	28
Tube inner diameter	mm	27
Length of tubes	mm	1084
Cooling water inlet temperature	°C	16
Maximum cooling water inlet temperature	°C	33
Cleanliness factor	-	0.85
Cooling water mass flow rate	kg/s	7697.61

EBSILON software can model various thermal systems under design and off-design conditions. The simulation is based on the principles of conservation of mass, energy, and momentum. The Gauss–Seidel iteration method, which is both fast and accurate, was selected for the calculation in EBSILON. Generally, the default iteration precision is 10^{-7}, and the maximum number of iterations is 999. The basic process of EBSILON modelling is shown in Figure 3. First, individual components are selected according to engineering requirements and combined into equipment units. Second, according to the system layout, the equipment units are connected in sequence to form a thermal system framework. Then, the parameters of different pipelines, such as mass flow rate, temperature and pressure, are set, and the internal parameters of the components are set to form a complete system model. Finally, a simulation calculation is performed using the model, and the calculation data are analysed. Figure 4 shows a model of the secondary circuit thermal system of the MHTGR power plant constructed using EBSILON software. The main components are marked, which correspond to those in Figure 1. Both the red and blue lines represent pipes, with the difference being the transported fluids, namely steam and water, respectively. The numbers 1–9 correspond to the nine distinct positions within the system, matching the numbers in Figure 5. To improve the precision of the model, steam leakage from the

shaft seals at all levels of the high- and low-pressure cylinders were considered during the modelling. Under 100% RC, the mass flow rate of the shaft seal steam leakage is 0.83 kg/s, accounting for approximately 0.45% of the main steam mass flow rate.

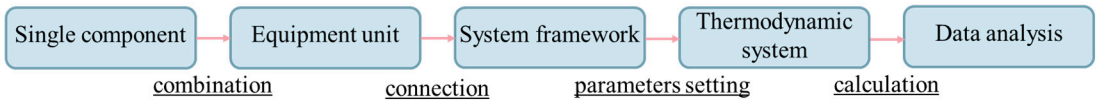

Figure 3. Modelling process in EBSILON software.

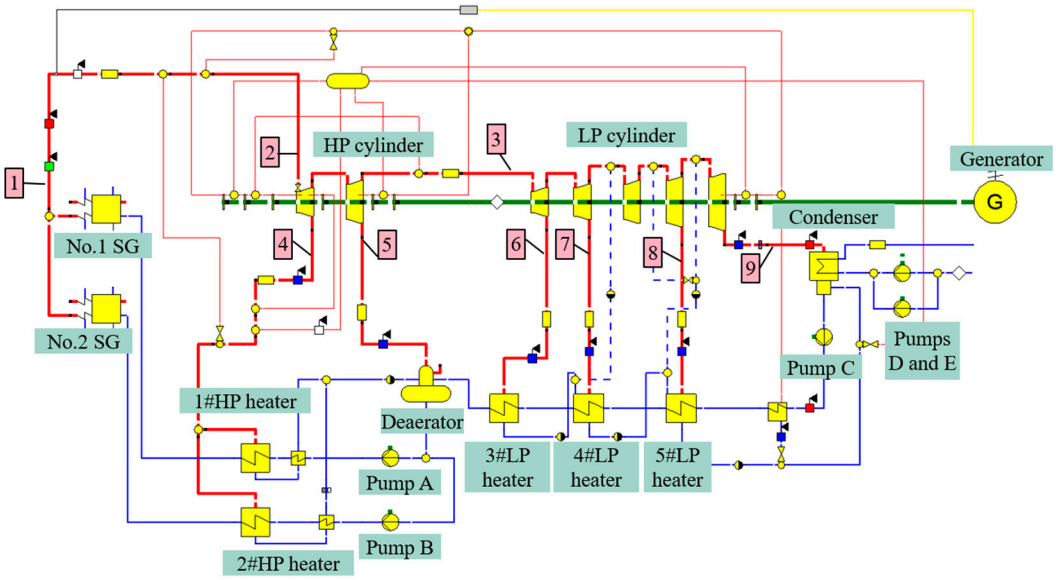

Figure 4. EBSILON model of the secondary circuit system of the MHTGR NPP.

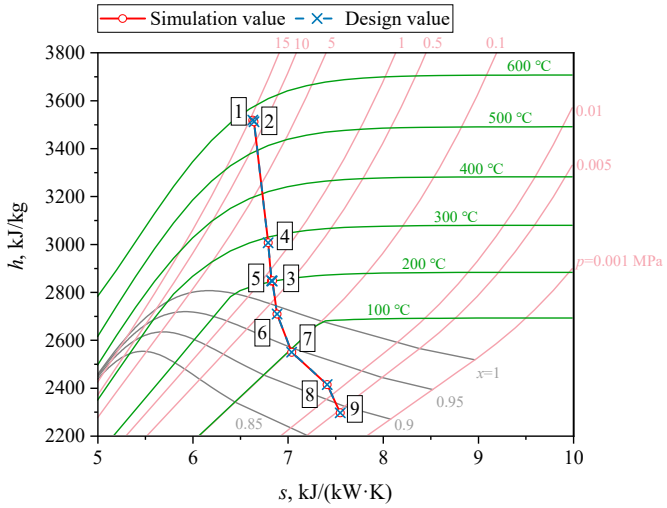

Figure 5. Enthalpy and entropy diagram of the steam expansion process in the steam turbine under 100% RC.

2.2. Model Validation

The quasi-steady-state simulations were conducted under typical operating conditions to verify the accuracy of the model. The simulation values were compared with the design values for the key parameters. The five typical operating conditions were 100%, 90%, 75%, 50% and 30% RC. In Figure 5; 2–5 represent the expansion process of steam in the HP cylinder, and 3–9 represent the expansion process of steam in the LP cylinders. The simulation values were mostly similar to the design values.

The EBSILON model employs a No. 39 component to determine the main steam mass flow rate under off-design conditions. One end of the component is connected to the generator to measure the gross power generation, whereas the other end is connected to the main steam header. The desired gross power generation can be manually set within the No. 39 component as the input under off-design conditions. The system then iteratively calculates the mass flow rate of the main steam required to achieve the target gross power generation. Table 3 lists three parameters, namely the main steam mass flow rate, main feed water temperature, and deaerator pressure, under five typical operating conditions, along with the relative errors between the simulation and design values. Table 4 displays the relative errors in the mass flow rate, pressure, and specific enthalpy of the extraction steam at the five regenerative extraction points I–V at 75% RC. For confidentiality reasons, the specific simulation and design values are not provided in Tables 3 and 4.

Table 3. Relative errors of different parameters under five typical operating conditions.

Operating Condition, % RC	Relative Error, %		
	Main Steam Mass Flow Rate, kg/s	Main Feed Water Temperature, °C	Deaerator Pressure, MPa
100	0	−0.01	0.00
90	−0.13	−0.04	−0.13
75	−0.56	−0.14	−0.38
50	−0.69	0.18	0.8
30	−2.98	−0.19	−0.57

Table 4. Relative errors of extraction parameters at extraction points under 75% RC.

Extraction Point	Relative Error, %		
	Mass Flow Rate, kg/s	Pressure, MPa	Specific Enthalpy, kJ/kg
I	−0.88	−0.54	−0.01
II	−0.37	−0.38	0.00
III	−0.69	−0.51	0.00
IV	−1.03	−0.48	−0.11
V	0.11	2.42	0.06

The results presented in Figure 5, Tables 3 and 4 demonstrate that the model performed well under five typical operating conditions: 100%, 90%, 75%, 50%, and 30% RC. The simulated values are closely aligned with the design values for the MHTGR NPP. Except for the individual parameters, the relative errors of the simulated values of the main parameters were within 1%. Therefore, the model established in this study was verified and could be used in subsequent studies.

3. Mathematical Model

Mathematical models of the condenser and pump were developed. The thermal performance evaluation indicators of the system include the net power, cycle efficiency, and heat consumption rate, each with specific definitions and formulas provided in Section 3.3. The prerequisites for the simulation experiments in this study are detailed in Section 3.4.

3.1. Condenser

In accordance with the law of energy conservation, the heat transfer rate of condenser $\dot{Q}_{CON}$ can be expressed as:

$$\dot{Q}_{CON} = \dot{m}_{CW}(h_{CW,out} - h_{CW,in}) = \dot{m}_{CON}(h_{CON,in} - h_{CON,out}). \quad (1)$$

where $\dot{m}_{CW}$ and $\dot{m}_{CON}$ are the mass flow rates of the cooling water and exhaust steam flowing into the condenser, respectively; $h_{CW,in}$ and $h_{CW,out}$ represent the specific enthalpy of the cooling water at the inlet and outlet of the condenser, respectively; $h_{CON,in}$ and

$h_{CON,out}$ are the specific enthalpy of the exhaust steam flowing into the condenser and condensate flowing out of the condenser, respectively.

The end temperature difference (δT) and logarithmic mean temperature difference ($LMTD$) are crucial indicators for assessing the condenser's heat transfer performance [28,29]. The condenser end temperature difference refers to the variance between the saturated steam temperature of the condenser and the cooling water outlet temperature. Both indicators can be expressed as follows:

$$\delta T = T_{CON} - T_{CW,out}, \tag{2}$$

$$LMTD = \frac{(T_{CON} - T_{CW,in}) - (T_{CON} - T_{CW,out})}{\ln \frac{T_{CON} - T_{CW,in}}{T_{CON} - T_{CW,out}}}, \tag{3}$$

where T_{CON} refers to the steam saturation temperature in the condenser, and $T_{CW,in}$ and $T_{CW,out}$ are the cooling water temperatures flowing into and out of the condenser, respectively.

Condenser back pressure and steam saturation temperature satisfy the following formula [30,31]. It's an empirical formula that captures solely numerical relationship.

$$p_{CON} = 0.00981 \times \left(\frac{T_{CON} + 100}{57.66} \right)^{7.46}. \tag{4}$$

3.2. Pump

The isentropic efficiency of the pump can be described as:

$$\eta_i = \frac{h_{PU,i} - h_{PU,in}}{h_{PU,out} - h_{PU,in}}, \tag{5}$$

where $h_{PU,in}$ and $h_{PU,out}$ represent the specific enthalpy of water at the inlet and outlet of the pump in the actual process, respectively, and $h_{PU,i}$ indicates the specific enthalpy of water at the pump outlet in the ideal isentropic process. In this study, the isentropic efficiency of the main feed water pumps and condensate pump was 0.83, and that of the cooling water pumps was set to 0.8.

3.3. Evaluation Index

In this study, net power P_n was defined as the difference between the gross power generation of the power plant and the power usage of the main feed waters, condensate water, and cooling water pumps. This is expressed as follows:

$$P_n = P_g - (W_{PU,A} + W_{PU,B} + W_{PU,C} + W_{PU,D} + W_{PU,E}), \tag{6}$$

where A and B represent the two main feed water pumps; C represents the condensate pump and D and E represent the two cooling water pumps.

The cycle efficiency η_{cy} is the ratio of the net power to the thermal power input into the secondary circuit system, which can be calculated as:

$$\eta_{cy} = \frac{P_n}{\dot{Q}_{cy}}, \tag{7}$$

where $\dot{Q}_{cy}$ indicates the thermal power input to the secondary circuit system, that is, the heat absorption power of the secondary side of the steam generator.

The heat consumption rate q refers to the heat required by the turbo-generator unit to produce 1 kW·h of electric energy [28], which is an important index for measuring the thermal performance of a power plant and can be expressed as [31]:

$$q = 3600 \times \frac{\dot{Q}_{cy}}{P_n}. \quad (8)$$

3.4. Prerequisite

Simulation experiments were carried out based on the following prerequisites.

(1) Eight operating conditions (100%, 90%, 80%, 70%, 60%, 50%, 40%, and 30% RC) were selected for research. Under the same operating conditions, the thermal power input to the secondary circuit system and main steam mass flow rate remained constant.
(2) The pipeline pressure loss at extraction point I was set to 3%, whereas that for extraction points II, III, IV, and V was assumed to be 5% based on engineering experience.
(3) Water and steam thermal properties were determined according to the IAPWS-IF97 standard [32].
(4) Heat dissipation to the external environment from other components was neglected, in addition to the main steam header and condenser. The main steam underwent a reduction in temperature and pressure from 571 °C and 13.9 MPa at the steam generator outlet to 566 °C and 13.24 MPa, respectively, at the steam turbine inlet.

4. Results and Discussion

The study was divided into two parts, encompassing a power range of 30% to 100% RC, employing a control variable approach. In the first part, the cooling water mass flow rate was maintained constant at the design value of 7697.61 kg/s, while studying the influence of changing cooling water inlet temperatures within the range of 10–33 °C. The temperature range was determined based on the combination of industrial and local climatic conditions. In the second part, a constant cooling water inlet temperature was maintained at the design value of 16 °C, and the mass flow rate of cooling water was varied from 6000 to 14,000 kg/s to examine the influence of mass flow rate. Subsequently, under 100% RC, the mass flow rate corresponding to the maximum net power is defined as the optimal cooling water mass flow rate. This optimal mass flow rate is determined for various power levels of the MHTGR NPP, with the cooling water inlet temperature set at 16 °C. Both the cooling water inlet temperature and mass flow rate were simultaneously altered, leading to the creation of a three-dimensional surface diagram illustrating the net power change. Additionally, the optimal cooling water mass flow rate is determined separately for cooling water inlet temperatures of 16 °C and 33 °C, both under 100% RC.

4.1. Influence of Cooling Water Inlet Temperature

Figures 6 and 7 show how the condenser end temperature difference and logarithmic mean temperature difference changed with respect to the cooling water inlet temperature. The data indicate that with a growth in the cooling water inlet temperature, both the condenser end and logarithmic mean temperature differences decrease. Additionally, at a given temperature, the condenser end and logarithmic mean temperature differences decreased as the power level of the NPP decreased.

Figure 8 illustrates the variation in the condenser back pressure at varying cooling water inlet temperatures. With the rise in cooling water inlet temperature, the condenser back pressure increased across the various power levels. Notably, at a cooling water inlet temperature of 33 °C, there was a significant increase in the condenser back pressure. As an example, consider the case of 100% RC, where without changing the cooling water mass flow rate, the condenser back pressure reaches 10.8 kPa at a cooling water inlet temperature of 33 °C, signifying a substantial 139.79% increase from the design parameter of 4.5 kPa at an inlet temperature of 16 °C. An elevated condenser back pressure in the Rankine cycle

results in a higher exhaust steam temperature and enthalpy, leading to a decline in the cycle efficiency, as quantitatively demonstrated in Figure 9 and Table 5.

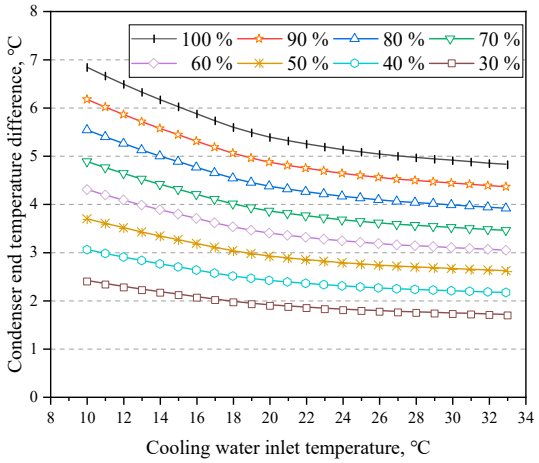

Figure 6. Variation of condenser end temperature difference with cooling water inlet temperature.

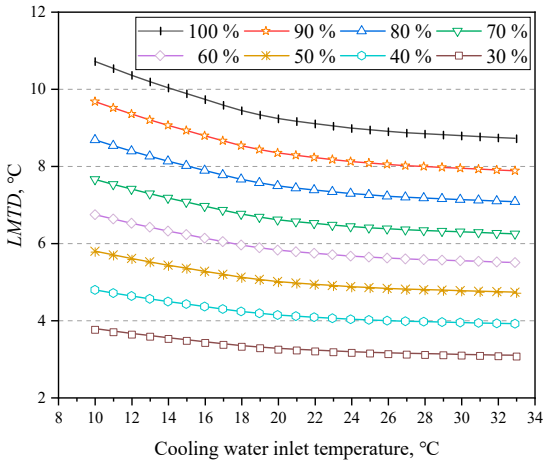

Figure 7. Variation of logarithmic mean temperature difference with cooling water inlet temperature.

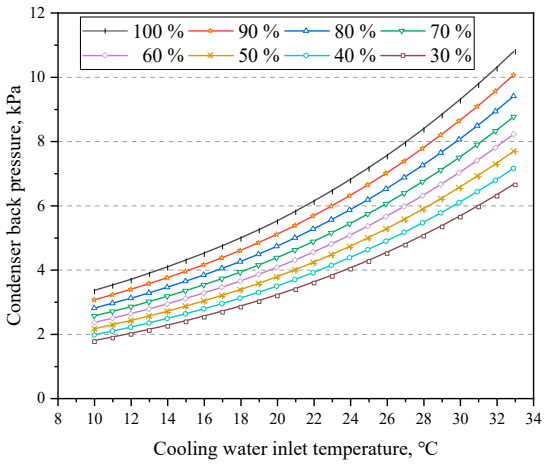

Figure 8. Variation of condenser back pressure with cooling water inlet temperature.

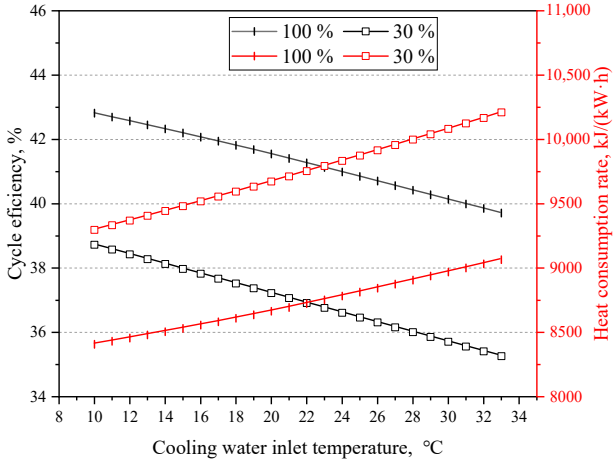

Figure 9. Cycle efficiency and heat consumption rate under 100% and 30% RC.

Table 5. Variation in cycle efficiency, heat consumption rate, and net power.

Operating Condition, % RC	Cooling Water Inlet Temperature, °C	Cycle Efficiency, %	Heat Consumption Rate, kJ/(kW·h)	Net Power, MW
100	10	0.75	−149.66	3.68
	33	−2.36	510.84	−11.64
30	10	0.90	−224.55	1.47
	33	−2.57	702.70	−4.18

As depicted in Figure 9, under 100% and 30% RC, the cycle efficiency exhibited a decline as the cooling water inlet temperature increased, whereas the heat consumption rate increased accordingly and the rate of change was approximately linear.

Figure 10 more comprehensively shows the change of unit net power with cooling water inlet temperature under 30–100% RC. Meanwhile, Table 5 displays the changes in cycle efficiency, heat consumption rate, and net power at cooling water inlet temperatures of 10 and 33 °C under 100% and 30% RC. These calculations are based on simulation results for a cooling water inlet temperature of 16 °C, the designated value for this parameter. The average value was then determined. Under 100% RC and within the temperature range of 10–33 °C, the system experiences a decrease of 0.67 MW in net power, a 0.14% reduction in cycle efficiency, and an increase of 28.72 kJ/(kW·h) in heat consumption rate for every 1 °C rise in the cooling water inlet temperature.

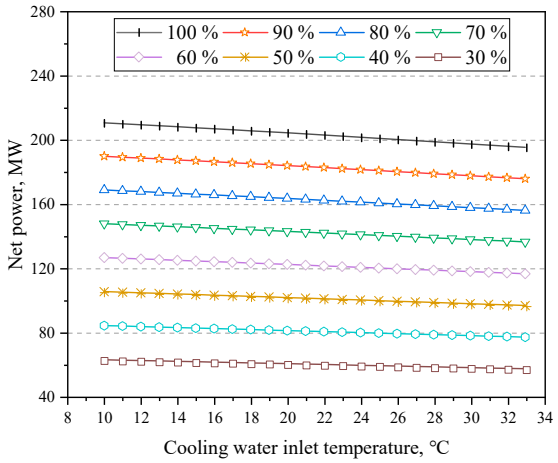

Figure 10. Variation of net power with cooling water inlet temperature.

Table 5 clearly illustrates the significant impact on unit net power when the cooling water inlet temperature reaches 33 °C without adjusting the cooling water mass flow rate.

Specifically, under 100% and 30% RC, the net power of the unit decreased by 11.64 and 4.18 MW, respectively. The reduction in net power can be attributed to the change in enthalpy drop during the steam expansion process. For instance, under 100% RC, the condenser back pressure was 4.5 and 10.8 kPa, respectively, when the cooling water inlet temperature was 16 and 33 °C. Additionally, the corresponding enthalpy drop during steam expansion work was 1219.39 and 1125.52 kJ/kg, respectively. Evidently, a higher cooling water inlet temperature resulted in a significant reduction in the enthalpy drop of the steam.

4.2. Influence of Cooling Water Mass Flow Rate

Figures 11–13 show the variations in the end temperature difference, logarithmic mean temperature difference, and back pressure of the condenser with respect to the cooling water mass flow rate. With the growth of the mass flow rate, the end temperature difference, logarithmic mean temperature difference, and back pressure of the condenser decreased under the eight operating conditions.

Although an increase in the cooling water mass flow rate results in a reduction in the condenser back pressure, which increases the gross power generation of the unit, an increase in the mass flow rate will lead to a rapid increment in the power consumption of the cooling water pumps, which will have an adverse effect on the net power of the NPP. Figure 14 shows the variation of net power with cooling water mass flow rate under 100% and 90% RC. The net power exhibits a clear trend, first increasing and then decreasing. This trend was consistently observed under the other operating conditions as well.

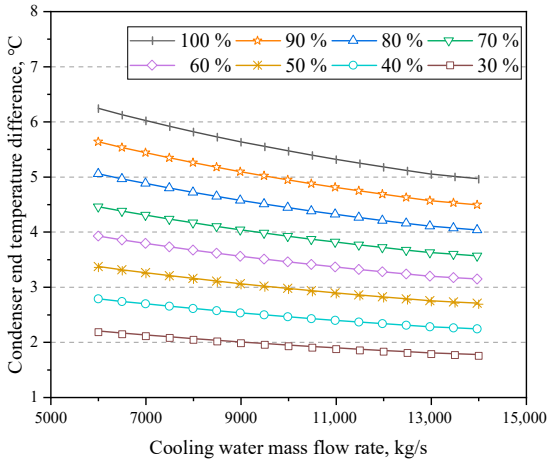

Figure 11. Variation of condenser end temperature difference with cooling water mass flow rate.

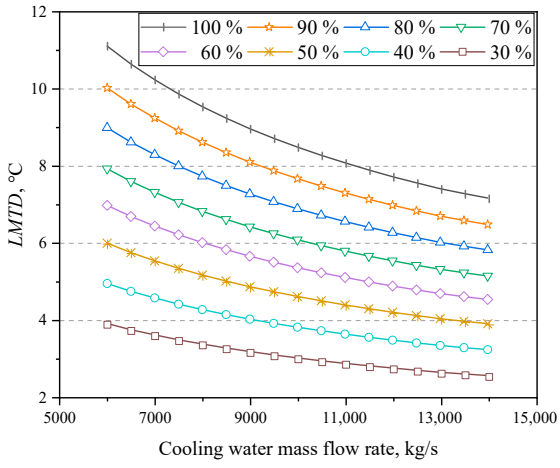

Figure 12. Variation of logarithmic mean temperature difference with cooling water mass flow rate.

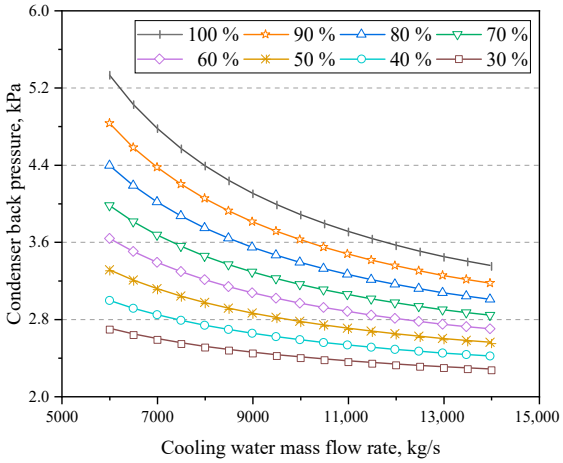

Figure 13. Variation of condenser back pressure with cooling water mass flow rate.

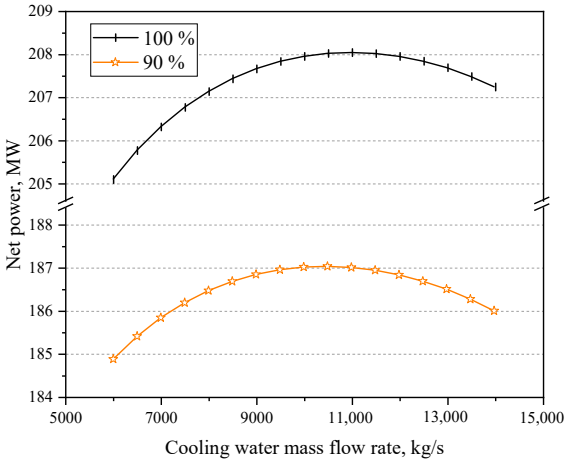

Figure 14. Variation of net power with cooling water mass flow rate under 100% and 90% RC.

Figure 15 shows the net power of the unit under eight operating conditions, where the red dotted line indicates the optimal mass flow rate of cooling water corresponding to the different power levels. As the power level decreased, the optimal cooling water mass flow rate gradually decreased, and the trend became nonlinear.

Figure 16 shows the variations in the cycle efficiency and heat consumption rate with cooling water mass flow rates under 100% and 30% RC. The net power exhibits a corresponding trend (Figure 17). When the mass flow rate increased, the cycle efficiency initially increased and then declined, whereas the heat consumption rate initially decreased and then increased. By adopting the optimal mass flow rate, the heat consumption rate was reduced by 46.11 and 15.18 kJ/(kW·h) at 100% and 30% RC, respectively. Furthermore, Figure 17 visually demonstrates the variation of the net power simultaneously with the cooling water inlet temperature and mass flow rate, aligning with the trends observed in Figures 10 and 15. At 33 °C and 6000 kg/s, the system's net power reached its minimum value of 193.57 MW.

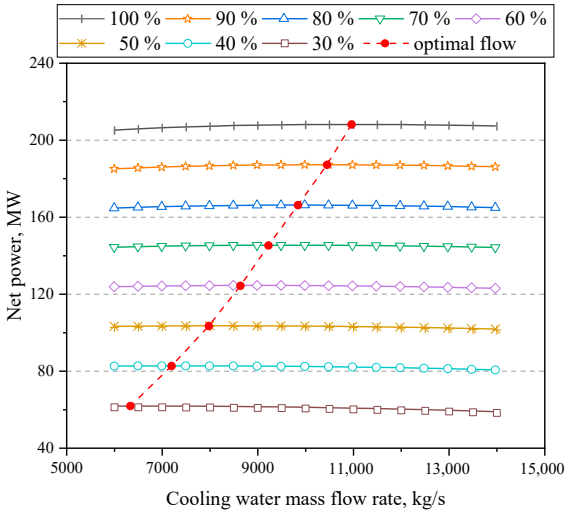

Figure 15. Net power changes with cooling water mass flow rate.

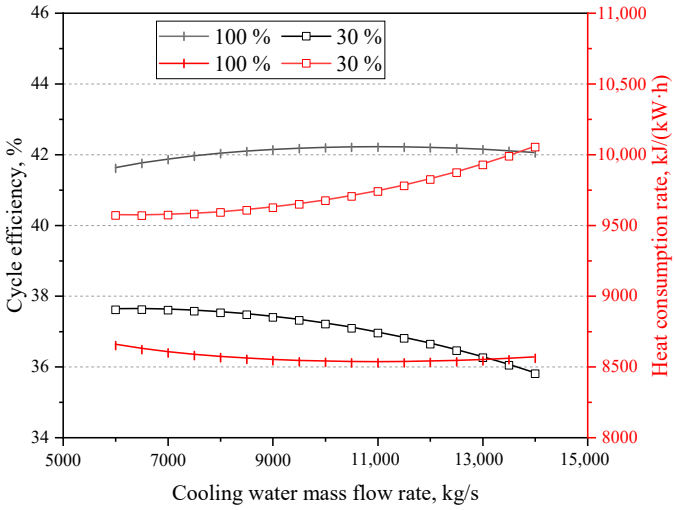

Figure 16. Cycle efficiency and heat consumption rate at 100% and 30% RC.

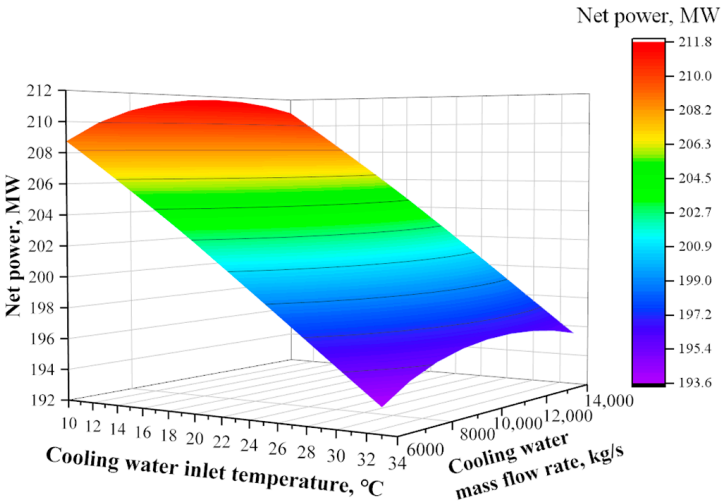

Figure 17. Influence of cooling water inlet temperature and mass flow rate on net power.

Figure 18 illustrates the net power increase of the unit under eight operating conditions when adopting the optimal cooling water mass flow rate. The green line represents the

design value of the cooling water mass flow rate of 7697.61 kg/s. The deviation between the optimal and design mass flow rates first decreased and then increased as the power level decreased. At higher power levels, the net power can be significantly improved by using the optimal cooling water mass flow rate. As an illustration, when the cooling water inlet temperature was 16 °C and the cooling water mass flow rate was reduced to the optimal mass flow rate under 30% RC, the unit's net power increased by 96.62 kW. This increase translates to an additional 96.62 MWh of electricity output for every 1000 h of operation at 30% RC. Furthermore, a comparison of Figure 18a,b reveals that the optimal cooling water mass flow rates under the two temperature conditions were relatively close.

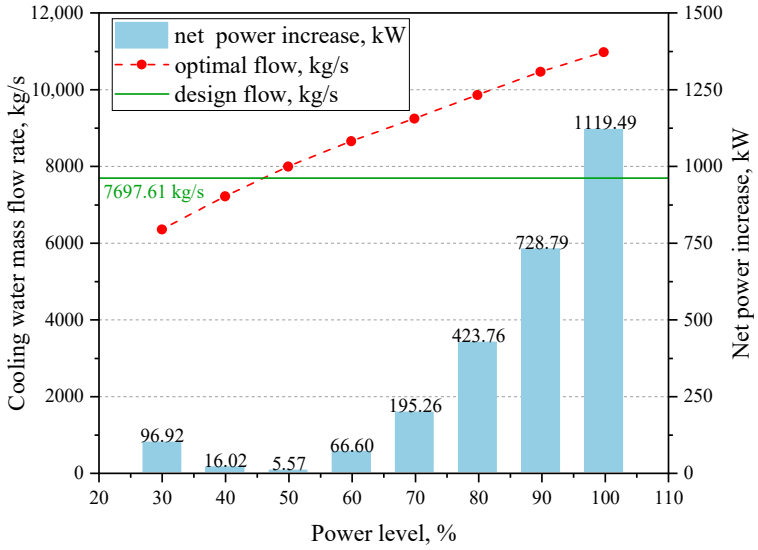

(**a**)

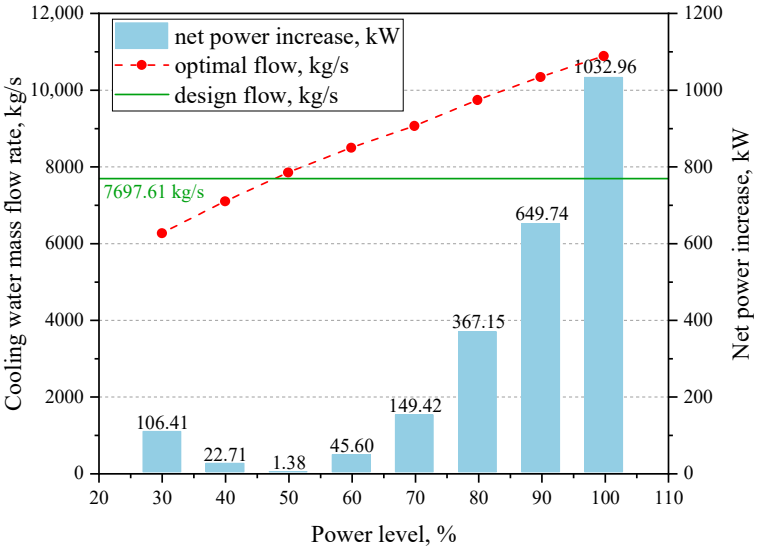

(**b**)

Figure 18. Net power increase under eight operating conditions. (**a**) $T_{CW,in}$ = 16 °C; (**b**) $T_{CW,in}$ = 33 °C.

5. Conclusions

The study utilised EBSILON software to establish and validate the thermal model of the secondary circuit in an MHTGR NPP. Variable operating condition simulations were performed across the full power range of stable operation of the NPP, using net power,

cycle efficiency, and heat consumption rate as thermal performance evaluation indicators. A wider spectrum of cooling water inlet temperatures was selected, and the effects of both the inlet temperature and mass flow rate on the system's thermal performance were studied in detail. Taking the maximum net power as the optimisation goal, the optimal cooling water mass flow rate for various power levels of the power plant was determined when the cooling water inlet temperature was 16 °C. Additionally, the optimal cooling water mass flow rate was determined for cooling water inlet temperatures of 16 °C and 33 °C under 100% RC. The following conclusions were drawn:

(1) Excessive cooling water inlet temperature causes a substantial elevation in condenser back pressure, resulting in a decline in the thermal performance of the unit. Particularly, at a cooling water inlet temperature of 33 °C, the condenser back pressure reached 10.8 kPa, which surpasses the design parameter of 4.5 kPa by a considerable 139.79%. Additionally, under both 100% and 30% RC, the net power decreased by 11.64 and 4.18 MW, respectively, and the cycle efficiencies decreased by 2.36% and 2.57%, respectively. Moreover, the heat consumption rate increased by 510.84 and 702.70 kJ/(kW·h). Furthermore, under 100% RC, a rise in the inlet temperature from 10 °C to 33 °C led to a reduction in the net power and cycle efficiency of the system by 0.67 MW and 0.14%, respectively, with the heat consumption rate escalating by 28.72 kJ/(kW·h) for every 1 °C increment.
(2) Within a certain range, the net power of the system first increased and then decreased as the cooling water mass flow rate increased. By considering the maximum net power as the optimisation goal, the optimal cooling water mass flow rate for various operating conditions can be determined. The findings indicated a nonlinear decrease in the optimal cooling water mass flow rate as the power level decreased.
(3) At a higher power level, appropriately increasing the cooling water mass flow rate can significantly increase the net power, whereas, at a lower power level, the cooling water mass flow rate must be reduced correspondingly to increase the net power. Taking cooling water inlet temperatures of 16 °C and 33 °C, respectively, when the mass flow rate increased from the design value to the optimal value under 100% RC, the net power increased by 1119.49 and 1032.96 kW, respectively.

In summary, this study demonstrated the qualitative and quantitative relationships between the cooling water parameters and evaluation indicators, providing a basis for evaluating the impact of high-temperature weather on the thermal performance of MHTGR NPPs. The optimisation of the cold-end system is a complex process that requires a comprehensive consideration of various factors and costs. This study considers maximum net power as the optimisation goal to obtain the optimal cooling water mass flow rate under different operating conditions, which can be used as a part of the cold-end system optimisation of MHTGR NPPs and provides a reference for power plant operation optimisation and economic improvement.

Author Contributions: Conceptualization, G.Z., X.Q. and X.Y.; methodology, G.Z., X.Q. and X.Y.; software, G.Z., X.Q. and X.W.; validation, X.W.; investigation, X.Q. and X.W.; resources, X.Q. and J.W.; data curation, X.W.; writing—original draft preparation, X.W.; writing—review and editing, X.Q.; supervision, X.Q. and P.W.; project administration, X.Q. and J.W.; funding acquisition, J.W. and X.Y. All authors have read and agreed to the published version of the manuscript.

Funding: This research was funded by the National Key R&D Program of China (Grant No. 2018YFB1900500), and LingChuang Research Project of China National Nuclear Corporation.

Data Availability Statement: Due to confidentiality requirements of the partner enterprise, the data used in this study are not publicly available. For access to the data related to this research, please contact the corresponding author.

Conflicts of Interest: No conflict of interest exists in the submission of this manuscript, and the manuscript is approved by all authors for publication.

Nomenclature

h	specific enthalpy, [kJ/kg]
$LMTD$	logarithmic mean temperature difference, [°C]
$\dot{m}$	mass flow rate, [kg/s]
T	temperature, [°C]
T_{CON}	steam saturation temperature in condenser, [°C]
p	pressure, [Pa]
p_{CON}	condenser back pressure, [kPa]
s	specific entropy, [kJ/(kg·K)]
q	heat consumption rate, [kJ/(kW·h)]
P_{n}	net power, [MW]
P_{g}	gross power generation, [MW]
W	power consumption, [MW]
$\dot{Q}_{\mathrm{CON}}$	condenser heat transfer rate, [kW]
$\dot{Q}_{\mathrm{cy}}$	thermal power input to the secondary circuit system, [MW]
Abbreviations	
HP	high-pressure
LP	low-pressure
RC	rated condition
Greek letters	
η_{cy}	cycle efficiency of the system, [%]
η_{i}	isentropic efficiency of the pump, [%]
δT	condenser end temperature difference, [°C]
Subscripts	
cy	cycle
CON	condenser
CW	cooling water
i	isentropic process
in	inlet
out	outlet
PU	pump

References

1. Doe, U.S. A Technology Roadmap for Generation IV Nuclear Energy Systems. In *Nuclear Energy Research Advisory Committee and the Generation IV International Forum*; Doene: Berryville, VA, USA, 2002; pp. 9–11.
2. Kugeler, K.; Zhang, Z. *Modular High-Temperature Gas-Cooled Reactor Power Plant*; Springer: Berlin/Heidelberg, Germany, 2018. [CrossRef]
3. Wang, J.; Ding, M.; Yang, X.; Wang, J. Performance comparison and optimization of two configurations of (Very) high temperature gas-cooled reactors combined cycles. *Ann. Nucl. Energy* **2016**, *94*, 279–287. [CrossRef]
4. Qu, X.; Zhao, G.; Wang, J. Thermodynamic evaluation of hydrogen and electricity cogeneration coupled with very high temperature gas-cooled reactors. *Int. J. Hydrogen Energy* **2021**, *46*, 29065–29075. [CrossRef]
5. Ni, H.; Qu, X.; Peng, W.; Zhao, G.; Zhang, P. Study of two innovative hydrogen and electricity co-production systems based on very-high-temperature gas-cooled reactors. *Energy* **2023**, *273*, 127206. [CrossRef]
6. Haneklaus, N.; Schröders, S.; Zheng, Y.; Allelein, H.-J. Economic evaluation of flameless phosphate rock calcination with concentrated solar power and high temperature reactors. *Energy* **2017**, *140*, 1148–1157. [CrossRef]
7. Gao, Q.; Zhang, P.; Sun, Q.; Zhang, P.; Chen, S.; Peng, W. Experimental and numerical investigation of sulfuric acid decomposition for hydrogen production via iodine–sulfur cycle. *Energy Convers. Manag.* **2023**, *289*, 117167. [CrossRef]
8. Lin, X.; Song, H.; Wang, L.; Guo, Y.; Liu, Y. Cold-end integration of thermal system in a 1000 MW ultra-supercritical double reheat power plant. *Appl. Therm. Eng.* **2021**, *193*, 116982. [CrossRef]
9. Wang, C.; Liu, M.; Zhao, Y.; Qiao, Y.; Chong, D.; Yan, J. Dynamic modeling and operation optimization for the cold end system of thermal power plants during transient processes. *Energy* **2018**, *145*, 734–746. [CrossRef]
10. Yang, J.; Zhang, R. Optimization for steam turbine cold-end system of a nuclear power plant and sensitivity analysis. *J. Nucl. Eng. Radiat. Sci.* **2017**, *3*, 014501. [CrossRef]
11. Ahmad, A.; Covatariu, A.; Ramana, M.V. A stormy future? Financial impact of climate change-related disruptions on nuclear power plant owners. *Util. Policy* **2023**, *81*, 101484. [CrossRef]
12. EDF. Annual Results 2022 Presentation. Available online: https://www.edf.fr/sites/groupe/files/2023-04/annual-results-2022-presentation-2023-02-17-v3-2.pdf (accessed on 28 July 2023).

13. Laskowski, R.; Theibech, M.; Uzunow, N. The effect of cooling water temperature on the performance of a BWR nuclear power plant. *Mod. Eng.* **2021**, *3*, 5–13. Available online: https://mengineering.eu/index.php/me/article/view/85/81 (accessed on 28 July 2023).
14. Attia, S.I. The influence of condenser cooling water temperature on the thermal efficiency of a nuclear power plant. *Ann. Nucl. Energy* **2015**, *80*, 371–378. [CrossRef]
15. Durmayaz, A.; Sogut, O.S. Influence of cooling water temperature on the efficiency of a pressurized-water reactor nuclear-power plant. *Int. J. Energy Res.* **2006**, *30*, 799–810. [CrossRef]
16. Laković, M.S.; Stojiljković, M.M.; Laković, S.V.; Stefanović, V.P.; Mitrović, D.D. Impact of the cold end operating conditions on energy efficiency of the steam power plants. *Therm. Sci.* **2010**, *14*, 53–66. [CrossRef]
17. Ahmadi, G.R.; Toghraie, D. Energy and exergy analysis of Montazeri Steam Power Plant in Iran. *Renew. Sustain. Energy Rev.* **2016**, *56*, 454–463. [CrossRef]
18. Medica-Viola, V.; Pavković, B.; Mrzljak, V. Numerical model for on-condition monitoring of condenser in coal-fired power plants. *Int. J. Heat Mass Transf.* **2018**, *117*, 912–923. [CrossRef]
19. Harish, R.; Subhramanyan, E.E.; Madhavan, R.; Vidyanand, S. Theoretical model for evaluation of variable frequency drive for cooling water pumps in sea water based once through condenser cooling water systems. *Appl. Therm. Eng.* **2010**, *30*, 2051–2057. [CrossRef]
20. Xia, L.; Liu, D.; Zhou, L.; Wang, P.; Chen, Y. Optimization of a seawater once-through cooling system with variable speed pumps in fossil fuel power plants. *Int. J. Therm. Sci.* **2015**, *91*, 105–112. [CrossRef]
21. Wang, W.; Liu, J.; Zeng, D.; Lin, Z.; Cui, C. Variable-speed technology used in power plants for better plant economics and grid stability. *Energy* **2012**, *45*, 588–594. [CrossRef]
22. Zhang, W.; Ma, L.; Jia, B.; Zhang, Z.; Liu, Y.; Duan, L. Optimization of the circulating cooling water mass flow in indirect dry cooling system of thermal power unit using artificial neural network based on genetic algorithm. *Appl. Therm. Eng.* **2023**, *223*, 120040. [CrossRef]
23. Laskowski, R.; Smyk, A.; Lewandowski, J.; Rusowicz, A.; Grzebielec, A. Selecting the cooling water mass flow rate for a power plant under variable load with entropy generation rate minimization. *Energy* **2016**, *107*, 725–733. [CrossRef]
24. Wu, T.; Wei, H.; Ge, Z.; Yang, L.; Du, X. Cooling water mass flow optimization for indirect dry cooling system of thermal power unit under variable output load. *Int. J. Heat Mass Transf.* **2019**, *133*, 1–10. [CrossRef]
25. Btaszczyk, A.; Gfuch, J.; Gardzilewicz, A. Operating and economic conditions of cooling water control for marine steam turbine condensers. *Pol. Mar. Res.* **2011**, *18*, 48–54. [CrossRef]
26. Laskowski, R.; Smyk, A.; Rusowicz, A.; Grzebielec, A. Optimization of the cooling water mass flow rate under variable load of a power unit. *Appl. Therm. Eng.* **2021**, *191*, 116874. [CrossRef]
27. Dong, L.; Zhou, Z. Simulation study on the condensing system of high-temperature reactor demonstration power station HTR-PM 200 based on Vpower. *Shenyang Inst. Eng. (Nat. Sci.)* **2011**, *7*, 16–19. [CrossRef]
28. Laskowski, R. Relations for steam power plant condenser performance in off-design conditions in the function of inlet parameters and those relevant in reference conditions. *Appl. Therm. Eng.* **2016**, *103*, 528–536. [CrossRef]
29. Laskowski, R.; Smyk, A.; Rusowicz, A.; Grzebielec, A. A useful formulas to describe the performance of a steam condenser in off-design conditions. *Energy* **2020**, *204*, 117910. [CrossRef]
30. Yang, T.; Wang, W.; Zeng, D.; Liu, J.; Cui, C. Closed-loop optimization control on fan speed of air-cooled steam condenser units for energy saving and rapid load regulation. *Energy* **2017**, *135*, 394–404. [CrossRef]
31. Feng, H.; Wang, M.; Wang, N.; Xu, Y.; He, S.; Gao, M. Influence of environmental parameters on the cold-end and thermal system of coal-fired power plant based on Ebsilon simulation. *Therm. Sci. Eng. Prog.* **2022**, *32*, 101340. [CrossRef]
32. *IAPWS-IF97*; Revised Release on the IAPWS Industrial Formulation 1997 for the Thermodynamic Properties of Water and Steam. The International Association for the Properties of Water and Steam: Oakville, ON, Canada, 2007.